3D Printed Abdominal Aortic Aneurysm Phantom for Image Guided Surgical Planning with a Patient Specific Fenestrated Endovascular Graft System

Karen M. Meess[*,a,b,c,d], **Richard L. Izzo**[a,c,d], **Maciej L. Dryjski**[e], **Richard E. Curl**[e], **Linda M. Harris**[e], **Michael Springer**[a], **Adnan H. Siddiqui**[a,d,f], **Stephen Rudin**[c,d,f,g], and **Ciprian N. Ionita**[c,d]

[a]The Jacobs Institute, Buffalo, NY 14203

[b]CUBRC Inc., Buffalo, NY 14225

[c]Department of Biomedical Engineering, University at Buffalo, Buffalo, NY 14228

[d]Toshiba Stroke and Vascular Research Center, University at Buffalo, Buffalo, NY 14203

[e]Department of Vascular Surgery, University at Buffalo Jacobs School of Medicine and Biomedical Sciences, Buffalo, NY 14203

[f]Department of Neurosurgery, University at Buffalo Jacobs School of Medicine and Biomedical Sciences, Buffalo, NY 14203

[g]Department of Radiology, University at Buffalo Jacobs School of Medicine and Biomedical Sciences, Buffalo, NY 14203

Abstract

Following new trends in precision medicine, Juxatarenal Abdominal Aortic Aneurysm (JAAA) treatment has been enabled by using patient-specific fenestrated endovascular grafts. The X-ray guided procedure requires precise orientation of multiple modular endografts within the arteries confirmed via radiopaque markers. Patient-specific 3D printed phantoms could familiarize physicians with complex procedures and new devices in a risk-free simulation environment to avoid periprocedural complications and improve training. Using the Vascular Modeling Toolkit (VMTK), 3D Data from a CTA imaging of a patient scheduled for Fenestrated EndoVascular Aortic Repair (FEVAR) was segmented to isolate the aortic lumen, thrombus, and calcifications. A stereolithographic mesh (STL) was generated and then modified in Autodesk MeshMixer for fabrication via a Stratasys Eden 260 printer in a flexible photopolymer to simulate arterial compliance. Fluoroscopic guided simulation of the patient-specific FEVAR procedure was performed by interventionists using all demonstration endografts and accessory devices. Analysis compared treatment strategy between the planned procedure, the simulation procedure, and the patient procedure using a derived scoring scheme.

Results—With training on the patient-specific 3D printed AAA phantom, the clinical team optimized their procedural strategy. Anatomical landmarks and all devices were visible under x-

---

[*]kmeess@jacobsinstitute.com; phone: 1 716 878 2432; fax: 1 716 854 1952; www.jacobsinstitute.com.

ray during the simulation mimicking the clinical environment. The actual patient procedure went without complications.

Conclusions—With advances in 3D printing, fabrication of patient specific AAA phantoms is possible. Simulation with 3D printed phantoms shows potential to inform clinical interventional procedures in addition to CTA diagnostic imaging.

Keywords

Abdominal Aortic Aneurysm (AAA); 3D Printing; Image Guided Intervention; Fenestrated EndoVascular Aortic Repair (FEVAR); Image Segmentation; Image Guided Procedure; Surgical Planning

1. INTRODUCTION

Rupture of Abdominal Aortic Aneurysms (AAA) is the 15th leading cause of death in the United States and 10th leading cause of death for men over the age of 55 in the United States [1, 2]. AAAs are characterized as a dilation of the abdominal aorta, one of the largest arteries in the body, which can rupture without warning resulting in life threatening bleeding. Rupture mortality rates reach 90%; only 50–70% of patients who survive long enough to receive an operation at the hospital recover [3, 4].

Therefore, the treatment strategy for patients diagnosed with AAAs is an elective aortic repair procedure with the goal of preventing rupture [5]. The current minimally invasive procedure is referred to as EndoVascular Aortic Repair stent grafting (EVAR), first documented in 1991[6]. This is a procedure in which a series of modular synthetic tubes with metal mesh supports are secured to the vessel proximal and distal to the aneurysm sac to create a new "pipe", preventing further growth and subsequent aneurysm rupture. Though effective, a substantial patient population is not eligible for EVAR due to the presence of an anatomical complexity characterized by a short proximal neck - less than 10 mm of normal aorta between the renal artery takeoff and aneurysm sac. This anatomical characteristic is inherent to a Juxtarenal Abdominal Aortic Aneurysm (JAAA), found in approximately 15% of AAA cases [5].

In 2012, the first stent graft designed for patients with JAAAs was approved (The Zenith® Fenestrated AAA Endovascular Graft, Cook Medical, Bloomington, IN). This device has small cut outs for the renal arteries and the superior mesenteric artery (SMA) which allows graft-vessel apposition at the proximal aneurysm neck, a type of placement not possible with standard EVAR grafts. As the takeoff angle and offset height of the renal arteries and SMA vary from patient to patient, this graft is custom-designed and manufactured for each case based on diagnostic CT Angiogram imaging (CTA) [7]. Due to the significant increase in complexity of procedures performed with this device compared to standard EVAR cases, the treatment of JAAAs is referred to by the name: Fenestrated EndoVascular Aortic Repair (FEVAR).

During stent graft treatment, anatomical complexities such as a short aneurysm neck (<10mm) and high vessel takeoff angle (among others) can result in difficulty achieving a

seal proximal and distal to the aneurysm. A poor seal results in a condition called endoleak where blood is still able to fill the aneurysm, potentially leading to further growth and subsequent rupture if not corrected [6, 8]. Endoleak can occur at the graft attachment sites to the vessel, branching arteries, or from a graft defect. The risk of poor proximal attachment has traditionally excluded JAAA patients from EVAR treatment, until the development of FEVAR [9]. These fenestrated stent grafts have a complex deployment process including: 1) critical image guided placement and deployment to ensure the fenestrations open to three major branching arteries of the abdominal aorta, 2) concurrent control of multiple catheter systems from up to three arterial access points, 3) coordinating overlap of five or six modular stent grafts to achieve a leak-proof system, depicted as a system in Figure 1 [7, 10].

Classically, physicians receive training for new, complex devices via Medical Device Manufacturer (MDM) programs such as clinical presentations, physician to physician training, or simulated use in benchtop *in vitro* phantoms. The later, benchtop *in vitro* models, are historically made of glass and/or silicone for their characteristics of transparency, robustness for multiple uses, and ability to facilitate image guided procedure simulation. The advent of additive manufacturing in recent years has resulted in the investigation of healthcare applications such as patient specific *in vitro* models.

Recent literature has highlighted the advancements in 3D printing allowing physicians to train and plan for procedures using patient-specific 3D printed models. Use of these phantoms to practice various approaches has shown promise as a method to improve clinical interventional training and reduce the risk of periprocedural complications. Patient specific AAA phantoms fabricated via additive manufacturing have been used to visualize complex anatomies and create models for mock graft deployment [11–14]. Previous investigations have traditionally been fabricated from stiff photopolymers that lack compliance of arteries vital for graft deployment. Many have followed this approach by fabricating a stiff 3D printed cast for silicone or polyurethane injection molding, creating systems to capture the flexible and compliant nature of the arteries [15–20]. However, this method is very time intensive, requiring days for molding, casting, and layering, in addition to producing phantoms with more rigid properties than human vasculature. In the last ten years, photopolymer additive manufacturing technology has advanced with the addition of commercially available flexible photoresins, namely the Stratasys Tango family. Several case studies have documented the feasibility of using 3D printed flexible photopolymers for AAA models, as well as initial quantification of material characteristics such as: compliance, stiffness, and pressure distributions [16, 17, 21].

In this study, we present a full-scale, flexible, patient-specific 3D printed phantom of abdominal and peripheral vasculature which has been used for X-ray guided vascular simulation of a FEVAR procedure. A physician preparing for his first FEVAR procedure was trained using all classical methods. In addition, a clinical simulation was performed two days prior to the procedure using the patient specific 3D printed phantom. Diagnostic CTA imaging, originally ordered for design of the patient specific FEVAR graft by Cook Medical, was used by biomedical engineers to design and fabricate a patient-specific 3D printed phantom. Through procedural simulation, the aims of the phantom were to: 1) visualize and acclimate the user to the unique FEVAR graft orientation techniques via radiopaque

markers, 2) practice modular endograft placement under fluoroscopy guided intervention, 3) rehearse and refine concurrent handling of the modular grafts and accessory devices, 4) identify potential failure modes in a risk-free clinical simulation.

2. METHODS AND MATERIALS

The AAA phantom fabrication process was based on the methodology defined by previous work of our laboratory to create anatomically accurate vascular structures. The key steps include: image acquisition, segmentation, STL mesh conversion, mesh cleanup and construction of support and flow structures, fabrication via additive manufacturing, and post processing [22–28]. Collection and analyses of all scan and patient data was covered under IRB approval.

2.1 Patient Profile

The patient is a 65-year-old male diagnosed with a Juxtarenal Abdominal Aortic Aneurysm (JAAA) through a CTA study. All available imaging and past medical history were evaluated by clinicians at the Gates Vascular Institute (Buffalo, NY) and the patient was deemed to be a suitable candidate for FEVAR treatment. After consultation with the medical team and family, the patient elected to undergo the FEVAR procedure.

2.2 Image Acquisition

CT images were acquired on a 320-slice Toshiba Aquilion One system with 0.742mm in-plane resolution and 2.5mm slice thickness. All available series were reviewed with physicians using the 3D Reconstruction capabilities of the Toshiba Vitrea (Toshiba Medical Systems Europe) workstation to quickly determine the diagnostic scan best suited for segmentation based on slice thickness, resolution, and clear tissue boundaries to identify the anatomic regions of interest: aortic lumen, thrombus, and calcifications. The CTA resulted in clear structure delineation, Figure 2.

2.3 Image Segmentation

The Vascular Modeling Toolkit (VMTK) was used to segment the arterial lumen, thrombus, and calcifications from the CTA imaging. In brief, the following procedure was performed: 1) a volume of interest was selected to limit the image data to only the region containing the aorta and associated structures, 2) the vascular lumen was segmented via a fast marching algorithm in which user specified seed and target points were identified, 3) a combination of thresholding and fast-marching methods were used to identify the thrombus surrounding the arterial lumen, 4) a pure thresholding step was used to isolate the pebbles of calcium which are embedded in the thrombus wall. After initializing each of the three regions, a geodesic active contours level set algorithm was employed to evolve the surface to zero-levels of the image gradient. The final step was to apply a standard marching cubes algorithm on the zero-level to construct a triangulated surface model of each component, which were individually written out to stereolithographic (STL) files for use in later steps. For a detailed overview of the segmentation methods employed here, please refer to our lab's prior publication[24].

2.4 Mesh Cleanup, Modification, and Construction of Flow Structures

Autodesk Meshmixer was used to clean up the mesh and remove artifacts from the segmentation process such as unclosed contours and jagged surfaces. For a detailed overview of this process, please refer to our lab's prior publications[23, 27].

The patient specific Zenith® FEVAR graft (Cook Medical, Bloomington, IN) for the patient procedure was manufactured with custom fenestrations based on diagnostic CTA imaging. As patient specific devices are relatively inaccessible for training purposes due to their cost and fabrication lead time, we slightly modified the patient anatomy with Meshmixer to ensure that a demonstration FEVAR graft would position and deploy with proper behavior. By maintaining patient specific geometry with minimal modifications, we aimed to provide the clinical intervention team with an *in vitro* model to train on the new procedure while also providing insight to possible patient specific challenges to inform the procedure. These modifications are described in Table 1, alongside patient and demonstration graft sizing specifications. The fenestrations are dimensioned based on angle of artery takeoff, a clock position, and distance from the top edge of the endograft, in millimeters.

Notable differences between the patient and demonstration graft dimensions include: 1) graft diameter, 2) right renal fenestration angle, 3) left renal fenestration angle and distance from edge. To ensure proper placement and deployment of the demo graft within the phantom, it was necessary to make modifications to the segmented anatomy. First, the aortic lumen was dilated 4 mm in the x–y direction to accommodate the 4 mm upsize of the demo graft. Second, the right renal artery was cut from the aorta, translated posterior 1 mm, translated superior 11 mm to match the demo graft distance from edge, and merged with the aorta. Lastly, the left renal artery was cut and translated 1 mm posterior. The thrombus and calcifications were dilated 4 mm as well to maintain the arterial lumen geometry. Figure 3 demonstrates these modifications.

Figure 4A–D details the stages of model smoothing and surface repair. The arterial lumen mesh was used to create a solid wall with a thickness of 2 mm with connectors at the arterial openings for attachment into a flow loop system, Figure 4E–F. The calcifications pebble the surface of the thrombus and arterial lumen, typical of AAAs. The thrombus outer surface was extruded 2 mm and made to attach to the lumen extrusion as a hollow chamber, which would eventually be filled with a viscous ultrasound gel, Figure 4F. Due to the Eden 260 print tray size constraints ($255 \times 252 \times 200$ mm), the phantom was printed in two segments for assembly with the final phantom shown in Figure 4G.

2.5 Additive Manufacturing and Post Processing

The final STL model was exported to a Stratasys Eden 260 3D printer. This single material printer is capable of printing 16 micron layers with a resolution of 20–85 microns for features below 50mm in size. The arterial and thrombus walls were printed with a photopolymer, FullCure 930 TangoPlus, an elastic material with a tensile strength similar to reported aortic vascular values, see Table 2 [29–31]. Support material was manually removed via waterjet and internal lumen flushing with catheters. After cleaning, separate pieces were adhered together with silicone glue to form the closed loop flow system. The thrombus

chamber was filled with ultrasound gel to mimic the pulsatile expansion of thrombus via a manually operated stopcock and syringe assembly. The final assembly is shown in Figure 4G.

2.6 Procedural Steps

EVAR procedures are typically performed in an operating room or an interventional radiology suite under general anesthesia. Physicians introduce devices to the femoral artery via percutaneous access [6]. An initial Digital Subtraction Angiography (DSA) run is captured to determine renal artery takeoffs to guide main body graft placement. The main body graft is then introduced and positioned just below the renal arteries at least 10 mm. The proximal portion is unsheathed, allowing the physician to perform final orientation so the iliac leg graft portions open towards their target arteries. After the main body graft is unsheathed, both distal ostia are accessed to allow modular deployment of the two separate iliac limb grafts. Finally, a compliant balloon is expanded at all modular graft overlaps to achieve a tight seal. A final angiography is performed to check for endoleak before removing all devices and closing the access points in the femoral artery.

FEVAR includes all EVAR procedural steps along with an additional set of complex actions to ensure maintained blood flow to the renal arteries and SMA, located in the proximal seal zone. These include: 1) precise placement of the proximal fenestrated graft, 2) renal stent placement, deployment, and flaring, 3) deployment of an additional endograft, known as the distal main body graft. The fenestrated proximal graft is unsheathed like the EVAR graft; however, precise orientation is vital to maintain blood flow to the renal arteries and SMA. Each small fenestration has four radiopaque gold markers, visible in Figure 1, and the fenestrated proximal graft has six radiopaque markers on opposite faces to confirm the anterior face of the graft is anterior via graft rotation. EVAR grafts are orientated with just two radiopaque triangles denoting iliac limb direction. Before complete deployment of the fenestrated proximal graft, the renal arteries are catheterized to ensure access. After deployment, renal stents are deployed with some overlap inside the proximal fenestrated graft and then flared at the graft interface with a balloon to avoid endoleak. Unlike EVAR, where proximal and distal regions are covered with one main body graft, FEVAR grafts are assembled with two components: the fenestrated proximal main body graft and the distal main body graft which bifurcates into the iliac limbs. It is crucial that overlap of these subcomponents is achieved to prevent endoleak. The presence of these additional complexities and procedural steps during FEVAR graft deployment - as compared with EVAR- results in additional potential failure modes and risk of periprocedural complications [32].

2.7 Experimental Setup

The mock procedure was performed under fluoroscopy guidance in a clinical training lab. To simulate blood flow, the phantom was connected to a Harvard Apparatus cardiac pulsatile pump set to 60 BPM and 35/65% systole/diastole ratio. Live fluoroscopy was performed via a Toshiba C-arm X-ray unit to allow the interventionists and support staff to clinically simulate device navigation and implantation. The only procedural modifications made were to artificially secure the sheaths in the femoral arteries to prevent leaking at the insertion

site. Figure 5 depicts the phantom connected within the flow loop system during the clinical simulation.

2.8 Image Guided Treatment Planning and Impact Scoring

To determine surgical planning impact, a novel scoring system was constructed to compare the planned treatment procedure (P1), with the surgical planning simulation procedure (P2), and with the patient interventional procedure (P3). In Stage P1, the physician and clinical support staff made a treatment plan based on patient diagnostic imaging, tabletop device demonstrations, and physician training sessions; which is a standard training regimen for new device procedures. Following treatment outline construction, the patient procedure was scheduled and the patient-specific device was ordered from Cook Medical. Typically, the physician would simply review the case and perform the procedure. However, here the physician performed a mock simulation using his treatment plan, P1, on the patient-specific phantom as he planned to on the actual patient. We recorded simulation procedural steps as P2, noting many "on-the-fly" treatment plan changes due to challenges that could only present themselves in a physical procedure. Two days after the simulation, the actual procedure steps during the patient's case were recorded as P3.

To quantify impact, alterations or deviations in treatment strategy from procedural plan to simulation procedure, P1–P2, and the simulation procedure to the patient procedure, P2–P3, were tracked for the ten most critical procedural steps vital for FEVAR success, identified by the clinical team and engineer. If there were deviations in treatment strategy such as technique, approach, or use of a different medical device, then a score of 1 was given. If the approach or device used was identical between stages, then a score of 0 was given. A score was assigned as 1 automatically where the interventionist was 1) practicing new device techniques, 2) comparing various devices to make informed treatment decisions, 3) in instances where excess time and care was spent as only possible in a simulation. Each set of scores were summed and normalized to the total number of critical procedure steps to obtain the scores denoted as P1–2 and P2–3. Thus, a score of 0 (zero) in P1–2 means that nothing changed; the treatment plan was identical with the treatment in the phantom simulation. A score of 1 (one) means that all key procedural steps changed. An example is depicted in Figure 6, One can also think about the planned case, P1, as the plan the physician would have attempted on the patient; The simulation, P2, as "Plan A", the actual set of events the physician would have performed on the patient sticking as much as possible to his plan, P1, but making adjustments as needed depending on procedural complications.; and the actual patient case as "Plan B" as the physician had the opportunity to adjust the plan to avoid newly-known complications and/ or challenges in the simulation but once again having to make adjustments "on the fly" to deal with arising challenges. Thus, performing a simulation could allow the physician to pass completely over Plan A and on to Plan B to maximize patient procedure success.

3. RESULTS

3.1 3D Printed AAA Phantom Fabrication

The 3D printed phantom was successfully manufactured, cleaned, and assembled, as illustrated in Figure 7. Phantom cost was $254.49, with a print time of approximately 13 hours, Table 3 depicts these resources. FullCure 930 TangoPlus, the photopolymer resin of the phantom, has documented material tensile strength in the range of abdominal aortic aneurysm lumen wall tissue, which has lower values than healthy aortic wall tissue, Table 2. Future multimaterial phantoms could incorporate these various properties distributed throughout the aortic wall based on morphology.

3.2 3D Printed Phantom Performance and Clinical Simulation

The phantom successfully maintained physiologic pressure supplied by the Harvard Apparatus cardiac pump with pulsatile flow patterns evidenced by contrast injection imaging and phantom pulsatile motion. Under fluoroscopy the aortic lumen and thrombus sac could be distinguished. The simulation took approximately 3.5 hours. Figure 8A–J depicts fluoroscopic imaging for each of the ten notable procedure steps in the 3D printed phantom.

3.3 Clinical Procedure and Simulation Impact Scoring

Fluoroscopic images are shown side by side in Figure 9 for comparison between the 3D printed phantom simulation (left) and the patient procedure (right). Figure 9A–B depict renal artery access, step 4, with guidewires and diagnostic catheters advanced into the renal arteries. Figure 9C–D depict the distal portion of the fenestrated endograft within the aneurysm sac and surrounding tissues. Clarity of the aneurysm lumen and devices is an apparent difference between the *in vitro* and *in vivo* imaging due to anatomical obstructions of the vertebrae, pelvis, and gastrointestinal tract *in vivo*. Figure 9E–F depict distal graft access, step 7. The irregular balloon shape upon expansion indicates that the balloon and guidewire are within distal graft, serving as confirmation that a limb graft will correctly overlap with the distal main body graft upon advancement.

Table 4 summarizes the impact of the critical procedural steps from procedural planning to simulation procedure, P1–2, and from the simulation procedure to the patient procedure, P2–3, per the impact scoring rules we devised. During the simulation, three of ten vital procedure steps had a change in approach. In addition, there were four additional procedural steps that the clinical team spent a significantly longer amount of time and radiation performing than would be acceptably exposed to a patient. During this time, the physician and clinical specialists discussed the patient specific endograft design, performed extensive imaging from various orientations to ensure correct graft orientation, and discussed possible device failures with imaging to identify possible periprocedural complications to be alert for and how to correct. Seven of ten, 70%, notable procedural steps were impacted from the planned procedure based on CTA imaging to the simulation on the 3D printed phantom with actual devices.

Fenestrated proximal graft deployment, step 3, resulted in graft torqueing upon the delivery system and top cap interference with the proximal graft ostium due to complex handling. All

portions of the graft handle must be moved in synchronization with one another to prevent graft over-torqueing which results in poor visual delineation of the radiopaque markers and possible incorrect graft delivery. In regards to the top cap retrieval, the distal graft sheath must be carefully observed concurrent with retraction to prevent collision with the implanted graft, often requiring minute corrections live-time. Failure of this step can result in graft dislodgement.

Renal artery access, procedure step 4, was more challenging than expected from viewing the diagnostic CTA imaging. The physician had to use multiple different shaped catheters and guidewires to advance the catheter into the right renal artery. Significant time was spent navigating the guidewire and catheter system under fluoroscopy compared with the left renal artery.

Renal artery stent deployment and flaring, procedure step 5, with the planned renal stent size resulted in too little of an overlap with the fenestrated proximal graft requiring a second stent implant for the right renal artery. Thus, the clinical team decided to use a larger size renal stent for the patient procedure to ensure enough graft overlap. In addition, specific training was performed by the scrub tech for proper balloon inflation and deflation technique required for renal stent flaring as the technique requires slow deflation, which is not typical.

During the patient procedure, P3, only one notable procedural step had a change in plan from the simulation, P2. Renal artery access was challenging, as it was in the 3D printed phantom, resulting in the use of multiple different shaped catheters, not used in the simulation, and imaging orientations for successful access. In addition, there was one step that required extensive time and technical discussion, fenestrated proximal endograft placement, and was automatically assigned a score of 1 as per our scoring system discussed. Endograft orientation was confirmed with various techniques to ensure the endograft would unsheathe in the proper orientation. Out of the ten notable procedural steps, 20% were deviated from the simulation to the patient procedure.

4. DISCUSSION

This work demonstrates the feasibility of fabricating 3D printed patient specific phantoms of JAAAs. The *in vitro* patient specific phantom proved to be useful for device training and pre-surgical planning using fluoroscopic image guidance. The modifications of the patient anatomy to ensure correct demonstration graft deployment was successful as the clinical team effectively trained on the use of the FEVAR graft and identified patient specific challenges. By using a demonstration graft with a slightly altered patient-specific phantom, training for clinical teams is more accessible, yet still can provide the benefits of patient-specific simulation. Ultimately these phantoms could be used for more patient-specific device training and personalized medicine surgical planning.

Patient specific phantom design was successful; however, the segmentation accuracy is limited by the resolution of the CTA imaging, in our case 3.0 mm thick slices which had to be smoothed in mesh cleanup. During fabrication, the Eden 260 was the only 3D printer available at the time. This limited the design to a single material and a limited build tray size

resulting in multiple modular pieces to maintain the 1:1 scale between the phantom and patient anatomy. The tensile strength of the 3D printed material, FullCure 930 TangoPlus, is within the range of arterial tissue as evident in Table 2, although the calcification properties could not be mimicked with the single material polyjet printer. Digital multi-material 3D printing will allow for multiple materials to be printed within the same phantom, allowing for distinct properties between healthy arterial wall, aneurysm arterial wall, and the calcifications; as an example of current work of our laboratory. The use of ultrasound gel for thrombus simulation resulted in more flexibility than photopolymers can currently provide, however the casing of the chamber did not allow for physiological thrombus movement. Although it was helpful to see the thrombus anatomy via fluoroscopy, the anatomy did not impact the graft deployment performance. Clinicians usually infer the outside of the thrombus aneurysm sac by observation of the pebble like calcifications marking the surface. Future work could focus on incorporation of a thrombus simulant for training purposes for physicians with more realistic material properties.

The clinical impact scoring comparing the planned procedure versus the simulated case and the actual case resulted in 70% and 20% deviation in procedural strategy, for P1–2 and P2–3 respectively. These results show that there were more procedural changes made from the original planned procedure to the simulation, P1–2, than to the procedure, P2–3, including identification of possible complications during simulation such as: 1) the need for fenestrated graft realignment during deployment, 2) challenging positioning of a renal stent, 3) identification of the need for a longer renal stent post-deployment, and 4) the necessity to confirm distal body graft ostium access via balloon inflation prior to iliac limb graft advancement. The physician spent more time during the simulation, compared with the patient procedure, asking questions about the graft deployment and imaging techniques with the clinical staff and experimenting with possible device features. These impactful lessons require a surplus of time in a risk-free environment, which are not feasible in a patient procedure.

We hypothesized that there would be more treatment changes between the planned treatment procedure and the simulation procedure, P1–2, compared with the surgical planning simulation and the patient interventional procedure, P2–3, as the physician would have the chance to practice, experiment, and identify unknown challenges with the clinical simulation as is not possible with 2D diagnostic imaging alone. In this regard, the phantom serves as: 1) a diagnostic tool, 2) a training aide, and 3) a rehearsal tool to foresee possible periprocedural complications. Without the AAA phantom for simulation, interventionists would proceed directly to the procedure from the pre-treatment outline. Therefore, the use of a pre-surgical patient specific phantom allowed the physicians to rehearse and refine their planned approach, possibly avoiding periprocedural complications and extra time spent on device learning during the patient procedure which in turn can decrease radiation exposure to the patient and staff, decrease anesthesia and contrast agent exposure to the patient, reduce procedure time by avoiding "on the fly" treatment change, and decrease number of devices used. The use of a AAA patient-specific phantom demonstrated successful surgical procedure training and a resulting successful patient procedure.

5. CONCLUSION

With advancements in image processing and 3D printing technology, fabrication of patient specific models for pre-surgical planning by physicians and the clinical team is possible. We fabricated a patient-specific JAAA phantom and facilitated a clinical simulation of a FEVAR graft implantation procedure with continuous fluid flow and fluoroscopic guided imaging. Our clinical impact scoring technique concluded that simulation was more effective at planning for periprocedural challenges and complications than standard pre-surgical planning based on CTA diagnostic imaging alone. Future work will focus on improving realistic radiopacity of the phantom, optimizing physiological flow, and mimicking tissue material properties using multi-material 3D printing with the goal of training physicians on the use of complex devices and procedures.

Acknowledgments

References

1. Singh, MJ. Society for Vascular Surgery - Abdominal Aortic Aneurysm. Available: https://vascular.org/patient-resources/vascular-conditions/abdominal-aortic-aneurysm

2. Upchurch GR Jr, Schaub TA. Abdominal aortic aneurysm. Am Fam Physician. 2006; 73:1198–204. [PubMed: 16623206]

3. Kent KC. Clinical practice. Abdominal aortic aneurysms. The New England Journal of Medicine. 2014; 371:2101. [PubMed: 25427112]

4. Keisler B, Carter C. Abdominal aortic aneurysm. American family physician. 2015; 91:538. [PubMed: 25884861]

5. Hu Z, Li Y, Peng R, Liu J, Zhang T, Guo W. Experience With Fenestrated Endovascular Repair of Juxtarenal Abdominal Aortic Aneurysms at a Single Center. Medicine (Baltimore). 2016; 95:e2683. [PubMed: 26962769]

6. Walker TG, Kalva SP, Yeddula K, Wicky S, Kundu S, Drescher P, d'Othee BJ, Rose SC, Cardella JF. Clinical Practice Guidelines for Endovascular Abdominal Aortic Aneurysm Repair: Written by the Standards of Practice Committee for the Society of Interventional Radiology and Endorsed by the Cardiovascular and Interventional Radiological Society of Europe and the Canadian Interventional Radiology Association. Journal of Vascular and Interventional Radiology. 2010; 21:1632–1655. [PubMed: 20884242]

7. Zenith(R) Fenestrated AAA Endovascular Graft. Instructions for Use. 2012. Available: https://www.cookmedical.com/data/IFU_PDF/IFU-FU_V3.PDF

8. O'Mara JE, Bersin RM. Endovascular Management of Abdominal Aortic Aneurysms: the Year in Review. Current treatment options in cardiovascular medicine. 2016; 18:54. [PubMed: 27376647]

9. Bashir MR, Ferral H, Jacobs C, McCarthy W, Goldin M. Endoleaks After Endovascular Abdominal Aortic Aneurysm Repair: Management Strategies According to CT Findings. American Journal of Roentgenology. 2009; 192:W178–W186. [PubMed: 19304678]

10. Farber M. Current State and Future State of Fenestrated Technology. Endovascular Today. 2013 Supplement.

11. Perrin D, Badel P, Orgeas L, Geindreau C, du Roscoat SR, Albertini JN, Avril S. Patient-specific simulation of endovascular repair surgery with tortuous aneurysms requiring flexible stent-grafts. Journal of the mechanical behavior of biomedical materials. 2016; 63:86–99. [PubMed: 27344232]

12. Erbano BO, Opolski AC, Olandoski M, Foggiatto JA, Kubrusly LF, Dietz UA, Zini C, Marinho MM, Leal AG, Ramina R. Rapid prototyping of three-dimensional biomodels as an adjuvant in the

surgical planning for intracranial aneurysms. Acta Cir Bras. 2013; 28:756–61. [PubMed: 24316741]

13. Winder RJ, Sun Z, Kelly B, Ellis PK, Hirst D. Abdominal aortic aneurysm and stent graft phantom manufactured by medical rapid prototyping. J Med Eng Technol. 2002; 26:75–8. [PubMed: 12102326]

14. Markl M, Schumacher R, Kuffer J, Bley TA, Hennig J. Rapid vessel prototyping: vascular modeling using 3t magnetic resonance angiography and rapid prototyping technology. MAGMA. 2005; 18:288–92. [PubMed: 16369802]

15. Morris L, Stefanov F, Hynes N, Diethrich EB, Sultan S. An Experimental Evaluation of Device/ Arterial Wall Compliance Mismatch for Four Stent-Graft Devices and a Multi-layer Flow Modulator Device for the Treatment of Abdominal Aortic Aneurysms. European journal of vascular and endovascular surgery : the official journal of the European Society for Vascular Surgery. 2016; 51:44–55.

16. Cloonan AJ, Shahmirzadi D, Li RX, Doyle BJ, Konofagou EE, McGloughlin TM. 3D-Printed Tissue-Mimicking Phantoms for Medical Imaging and Computational Validation Applications. 3D Printing and Additive Manufacturing. 2014; 1:14–23.

17. de Galarreta SR, Aitor C, Antón R, Finol EA. Abdominal aortic aneurysm: from clinical imaging to realistic replicas. Journal of biomechanical engineering. 2014; 136:014502. [PubMed: 24190650]

18. Friedman MH, Kuban BD, Schmalbrock P, Smith K, Altan T. Fabrication of vascular replicas from magnetic resonance images. J Biomech Eng. 1995; 117:364–6. [PubMed: 8618391]

19. Lermusiaux P, Leroux C, Tasse JC, Castellani L, Martinez R. Aortic aneurysm: construction of a life-size model by rapid prototyping. Ann Vasc Surg. 2001; 15:131–5. [PubMed: 11265074]

20. Peattie RA, Golden E, Nomoto RS, Margossian CM, Pancheri FQ, Edgar ES, Iafrati MD, Luis Dorfmann A. A Technique for Comparing Wall Pressure Distributions in Steady Flow Through Rigid Versus Flexible Patient-based Abdominal Aortic Aneurysm Phantoms. Experimental Techniques. 2015 n/a-n/a.

21. Biglino G, Verschueren P, Zegels R, Taylor AM, Schievano S. Rapid prototyping compliant arterial phantoms for in-vitro studies and device testing. J Cardiovasc Magn Reson. 2013; 15:2. [PubMed: 23324211]

22. Ionita CN, Garcia VL, Bednarek DR, Snyder KV, Siddiqui AH, Levy EI, Rudin S. Effect of injection technique on temporal parametric imaging derived from digital subtraction angiography in patient specific phantoms. Proc SPIE Int Soc Opt Eng. 2014; 9038:90380L.

23. Ionita CN, Mokin M, Varble N, Bednarek DR, Xiang J, Snyder KV, Siddiqui AH, Levy EI, Meng H, Rudin S. Challenges and limitations of patient-specific vascular phantom fabrication using 3D Polyjet printing. Proc SPIE Int Soc Opt Eng. 2014; 9038:90380M.

24. Izzo RL, O'Hara RP, Iyer V, Hansen R, Meess KM, Nagesh SVS, Rudin S, Siddiqui AH, Springer M, Ionita CN. 3D printed cardiac phantom for procedural planning of a transcatheter native mitral valve replacement. Proc SPIE Int Soc Opt Eng. 2016 978908-978908-16.

25. Mokin M, Ionita CN, Nagesh SV, Rudin S, Levy EI, Siddiqui AH. Primary stentriever versus combined stentriever plus aspiration thrombectomy approaches: in vitro stroke model comparison. J Neurointerv Surg. 2015; 7:453–7. [PubMed: 24789594]

26. Mokin M, Setlur Nagesh SV, Ionita CN, Levy EI, Siddiqui AH. Comparison of Modern Stroke Thrombectomy Approaches Using an In Vitro Cerebrovascular Occlusion Model. American Journal of Neuroradiology. 2015; 36:547–551. [PubMed: 25376809]

27. O'Hara RP, Chand A, Vidiyala S, Arechavala SM, Mitsouras D, Rudin S, Ionita CN. Advanced 3D mesh manipulation in stereolithographic files and post-print processing for the manufacturing of patient-specific vascular flow phantoms. Proc SPIE Int Soc Opt Eng. 2016 978909-978909-10.

28. Russ M, O'Hara R, Setlur Nagesh SV, Mokin M, Jimenez C, Siddiqui A, Bednarek D, Rudin S, Ionita C. Treatment planning for image-guided neuro-vascular interventions using patient-specific 3D printed phantoms. Proc SPIE Int Soc Opt Eng. 2015 941726-941726-11.

29. Rangwala HS, Ionita CN, Rudin S, Baier RE. Partially polyurethane-covered stent for cerebral aneurysm treatment. J Biomed Mater Res B Appl Biomater. 2009; 89:415–29. [PubMed: 18837459]

30. PolyJet Materials Data Sheet. 2016

31. Wang DH, Makaroun M, Webster MW, Vorp DA. Mechanical properties and microstructure of intraluminal thrombus from abdominal aortic aneurysm. J Biomech Eng. 2001; 123:536–9. [PubMed: 11783723]

32. Glebova NO, Selvarajah S, Orion KC, Black JH Iii, Malas MB, Perler BA, Abularrage CJ. Fenestrated endovascular repair of abdominal aortic aneurysms is associated with increased morbidity but comparable mortality with infrarenal endovascular aneurysm repair. Journal of Vascular Surgery. 2015; 61:604–610. [PubMed: 25499706]
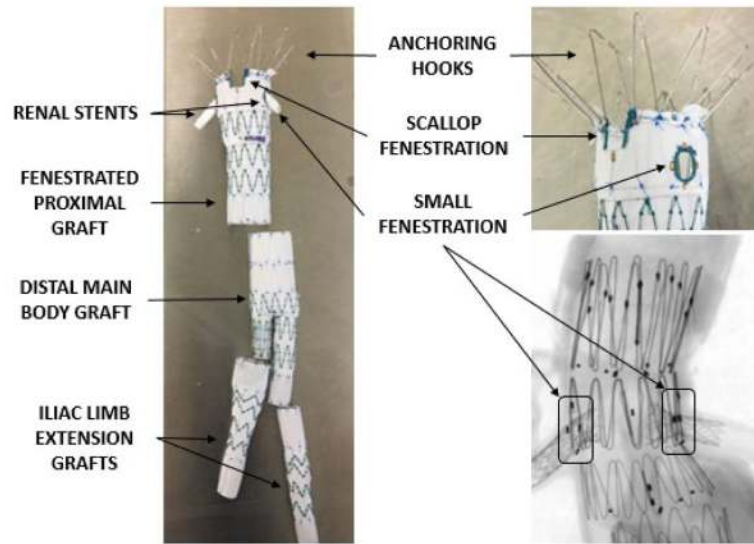
Figure 1.
FEVAR modular endograft device system, left, and fenestrated proximal endograft detail, right. Anchoring hooks secure the graft in the aorta upon deployment. Visible are the scallop and small fenestrations with four radiopaque gold markers stitched into the edge of each small fenestration with a visual depiction of the graft components under x-ray.
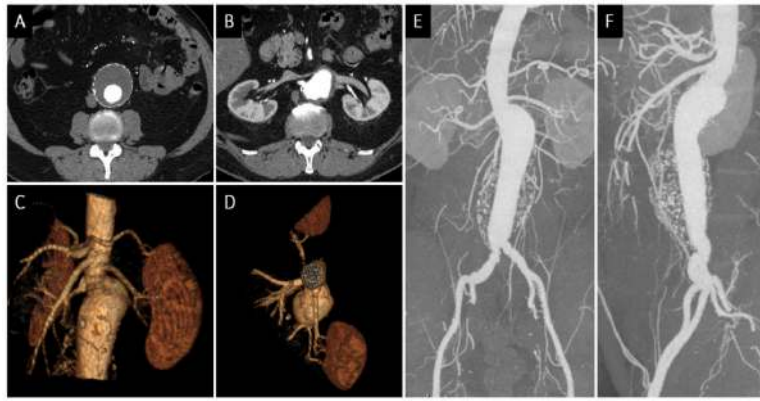
Figure 2.
Depictions of patient CTA diagnostic imaging including: transverse CTA slices depicting (a) distinction of arterial lumen, thrombus, and calcifications, and (b) renal artery takeoff from aorta to kidneys, 3D reconstructions depicting (c) JAAA posterior curve with visible left renal and SMA takeoffs, and (d) inferior view of takeoff angle for renal arteries and SMA, (e) coronal CTA slice with visible difference in renal artery heights as well as thrombus wall calcifications, and (f) sagittal CTA slice with visible posterior JAAA curve and thrombus wall calcifications.
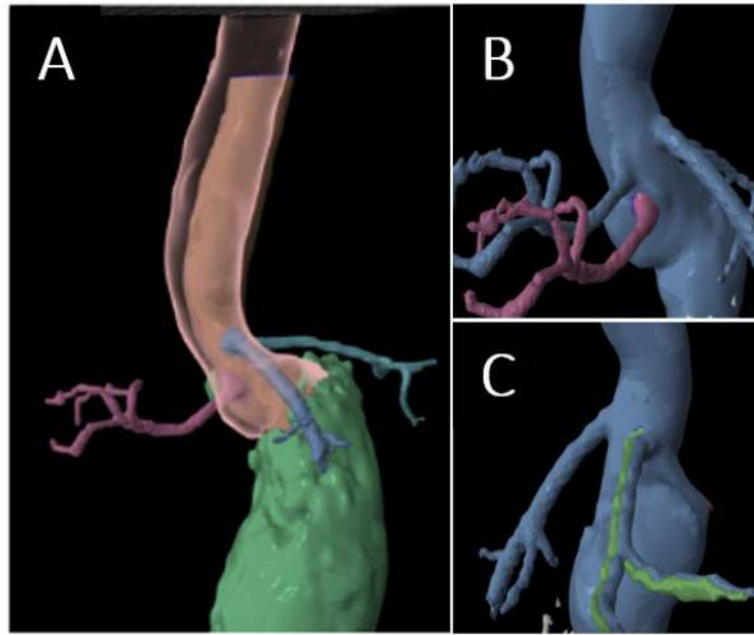
Figure 3.
Patient anatomy modifications for demo graft implantation: (a) dilated aorta (transparent red) compared to original arterial lumen (orange), (b) posterior and superior translation of the patient right renal artery (original location in pink), and (c) posterior translation of left renal artery (original location in green).
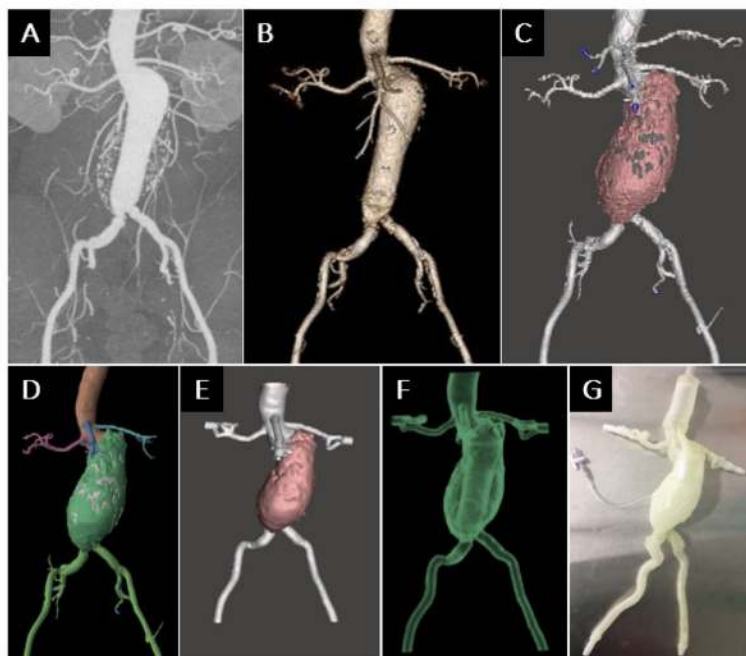
Figure 4.
AAA phantom fabrication process depicting (a) coronal CTA slice, (b) 3D reconstruction for diagnosis and initial treatment planning, (c) segmented arterial lumen (grey), thrombus (pink), and calcifications (dark grey) converted to STL meshes, (d) modified patient anatomy to fit demonstration fenestrated proximal graft dimensions, (e) final hollow phantom design with 2 mm wall thickness, (f) final hollow phantom design viewed as transparent, depicting the thrombus chamber, and (g) assembled AAA phantom.
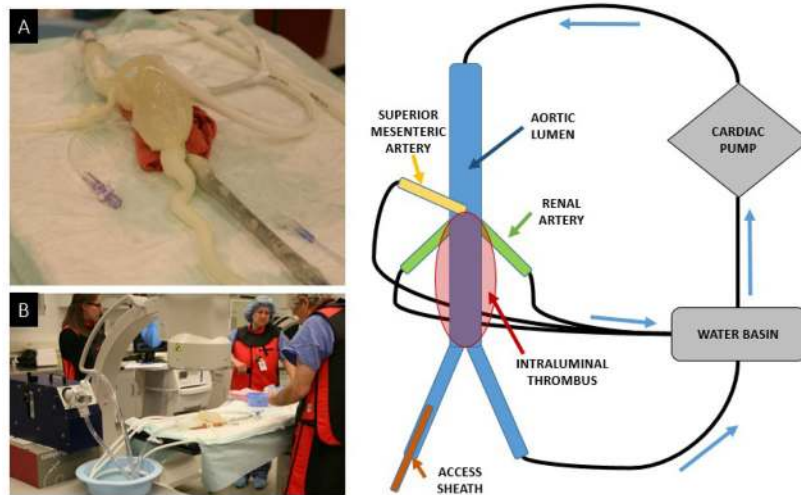
Figure 5.
Clinical simulation system design including: (a) assembled AAA phantom within the flow loop system, (b) simulation laboratory setup including cardiac pump, fluoroscopic imaging system, and clinical staff manipulating devices through the introducer sheath entry to the AAA phantom. System diagram, on right, depicts the fluid recirculation system into the abdominal aorta with outflows from the renal arteries, SMA, and iliac artery.
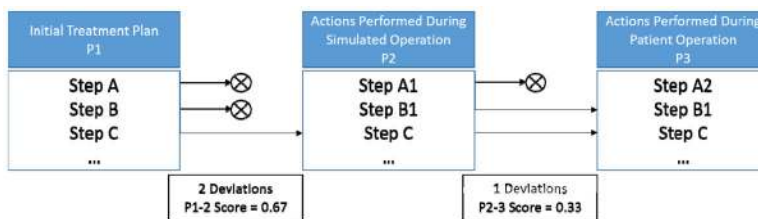
Figure 6.
Clinical impact scoring system representing the plan evolution of three example procedural steps (A, B, C) from the initial treatment plan through simulation and the patient procedure. The image depicts three steps that were planned during P1: Steps A, B, and C. During P2, two of those steps (67%), A and B, were not successful. The clinical staff had to try different approaches to be successful, marked as Steps A1 and B1 which became the new plan for the upcoming patient procedure. During P3, one step was unsuccessful (33%), resulting in a change in treatment approach, A2. However, the treatment step B1 which was discovered in the simulation was successful. Therefore, deviations in treatment strategy from the proposed plan at both the simulation and patient procedure can be tracked in this manner.
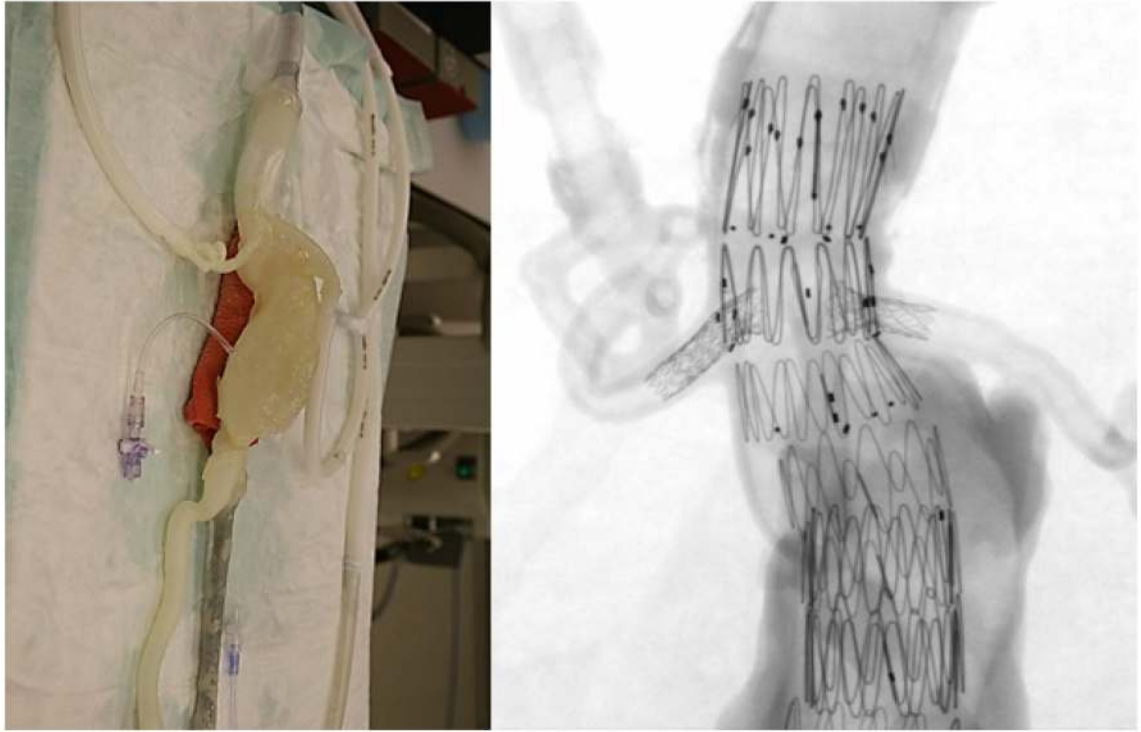
Figure 7.
Depiction of the final 3D printed phantom of the patient AAA. Image on left depicts the final phantom assembly within the flow loop experimental setup. Image on right is a fluoroscopic image of the 3D printed phantom post simulation. Evident are the proximal fenestrated graft, the top most portion of the distal main body graft and both renal grafts.
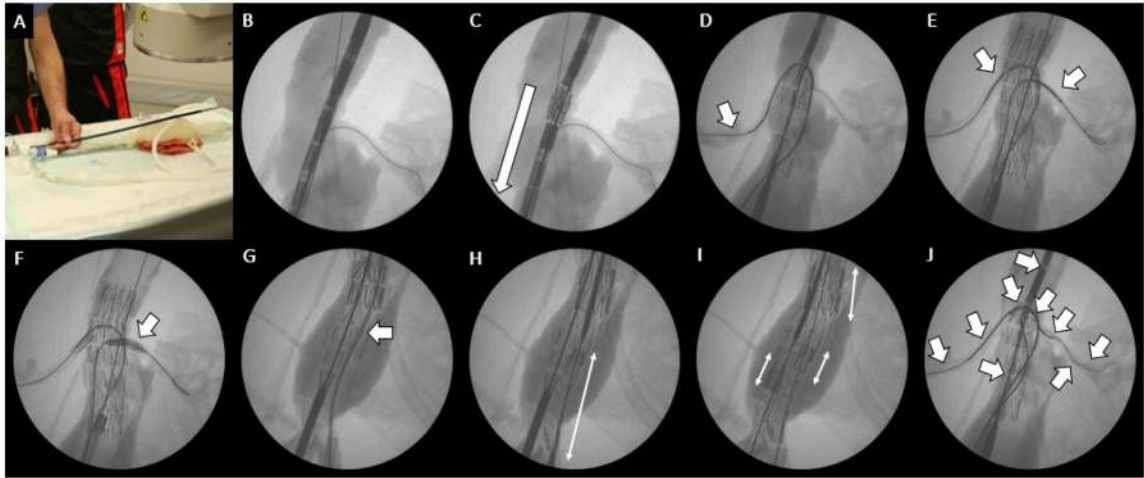
Figure 8.
Fluoroscopic imaging of the ten procedure steps: (a) introducer sheath insertion through the femoral artery to the aortic bifurcation, (b) fenestrated endograft placement via graft handle rotation and radiopaque marker visualization, (c) fenestrated endograft deployment along the direction of the arrow, (d) renal artery access with a wire and catheter assembly, arrow points towards catheterization of right renal artery, (e) renal artery stent placement accomplished via positioning of radiopaque stent struts slightly within the fenestrated endograft, two arrows, (f) renal artery stent deployment and flaring with a balloon, arrow indicates left renal stent expansion, (g) catheter and guidewire access within the distal main body graft ostium, arrow points to catheter successfully through gate, (h) sizing of a proper limb graft along the arrow line, (i) modular endograft overlap in the AAA phantom visualized by 3 arrows, and, (j) concurrent control of many devices from multiple access points, each arrow indicates an individual device present during endograft positioning, placement, and endograft overlap – total of nine devices used in one instance, not including the additional devices used for previous and proceeding steps.
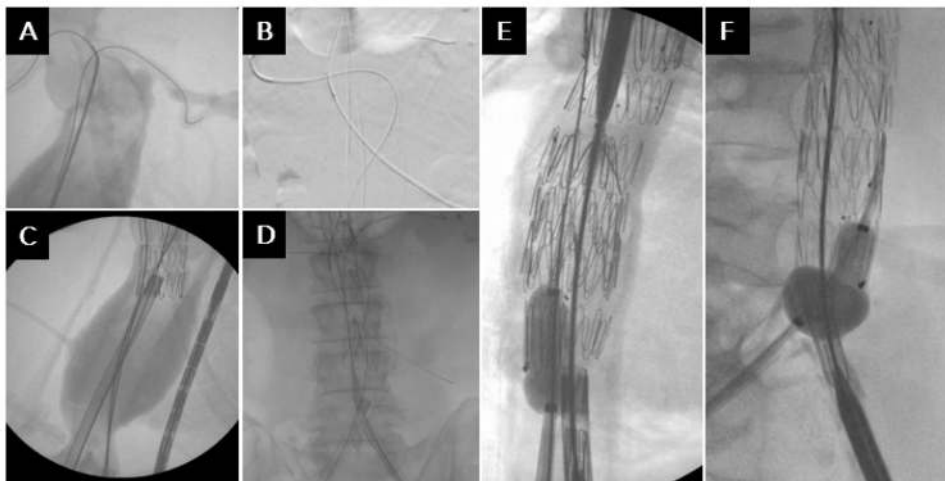
Figure 9.
Imaging comparison between 3D AAA phantom (left) and patient (right) depicting: (a–b) renal artery access with catheters and guidewires, (c–d) aneurysm and the surrounding tissue including vertebrae, pelvis, and GI tract in the patient, and (e–f) balloon inflation in the distal main body graft to confirm access through gate for subsequent iliac limb graft deployment. The patient imaging (b, d, f) evidences additional imaging obstructions such as the spinal vertebrae, pelvis, and GI tract which could make navigation and positioning of the devices more challenging *in vivo* than within the *in vitro* AAA phantom.

Table 1

Fenestrated graft dimensions of patient specific and demonstration grafts with associated phantom design modifications.

	Patient Graft	Demo Graft	Modifications to Patient STL
Vessel Diameter	23 mm	26 mm	Dilate aorta by 4–5 mm (x, y axes)
Graft Diameter	28 mm	32 mm	
Fen #1 (SMA)	Large Fen	Scallop	-
O' clock	12:00	12:00	N/A
Distance from Edge	11 mm	H - 10 mm W - 10 mm	N/A
Fen #2 (Right Renal)	Small Fen	Small Fen	-
O' clock	10:00	9:00	Cut and translate right renal posterior and lateral by 1 mm
Distance from Edge	26 mm	15mm	Translate the right renal superior to be 15 mm below SMA
Fen # 3 (Left Renal)	Small Fen	Small Fen	-
O' clock	2:00	3:00	Cut and translate the left renal posterior and lateral by 1 mm
Distance from Edge	15 mm	15 mm	N/A

Table 2

Comparison of 3D print materials to tissue values reported in literature.

Material	Longitudinal Tensile Strength [N/cm^2]	Source
Abdominal Aortic Wall	201.4 ± 39.4	Raghavan and Vorp[31]
Abdominal Aortic Aneurysm Wall	86.4 ± 10.2	Raghavan and Vorp[31]
FullCure 930 TangoPlus	80–150 (0.8–1.5MPa)	Stratasys[32]
Intraluminal Thrombus	52 ± 7	Wang and Vorp[33]

Table 3

3D Printing resources required for fabrication of the AAA phantom

Model	Material Cost	FullCure 930 TangoPlus [grams]	Support 705 [grams]	Print Time [hours:minutes]
AAA	$182.23	325	566	8:47
Iliac and Femoral Arteries	$44.22	88	114	2:53
Total	**$226.45**	**413**	**680**	**11:40**

Table 4

Impact Scores from Planned Procedure to Simulation (P1–2) and Simulation to Patient Procedure (P2–3)

	Notable Procedure Step (*Instructions for Use Step #*)	Procedural Step Deviation	
		P1–2	P2–3
1	Aortic Bifurcation Access with 20 Fr Sheath *(11.4.4)*	0	0
2	Fenestrated Endograft Placement *(11.4.5.5)*	1 *	1 *
3	Fenestrated Endograft Deployment *(11.4.5.8–9)*	1 †	0
4	Renal Artery Access *(11.4.5.10–11)*	1 †	1 †
5	Renal Artery Stent Placement (*11.4.7.1–2*)	1 †	0
6	Renal Artery Stent Deployment and Flaring *(11.4.7.3–5)*	1 *	0
7	Access to distal graft leg opening *(11.4.9.1)*	1 *	0
8	Sizing of Iliac Graft *(11.4.11)*	0	0
9	Prevention of Endoleak with Overlap *(13.1.14)*	0	0
10	Awareness and Control of All Concurrent Devices *(All Steps)*	1 *	0
	Procedural Step Deviation Scores	**P1–2 = 0.70**	**P2–3 = 0.20**

†
Change in treatment plan or approach

*
A score was assigned as 1 automatically where the interventionist was 1) practicing new device techniques, 2) comparing various devices to make informed treatment decisions, 3) in instances where excess time and care was spent as only possible in a simulation